IET Research Journals

Submission Template for IET Research Journal Papers

IET Journals
The Institution of Engineering and Technology

ISSN 1751-8644
doi: 0000000000
www.ietdl.org

Direct path interference suppression for short range passive bistatic SAR imaging based on atomic norm minimization and Vandermonde decomposition

Weike Feng[1], Jean-Michel Friedt[2], Grigory Cherniak[1], Zhipeng Hu[3], Motoyuki Sato[4]*

[1] *Graduate School of Environmental Studies, Tohoku University, Sendai, Japan*
[2] *Time and Frequency department, FEMTO-ST, Besancon, France*
[3] *College of Geoexploration Science and Technology, Jilin University, Changchun, China*
[4] *Center for Northeast Asian Studies, Tohoku University, Sendai, Japan*
** E-mail: feng.weike.q4@dc.tohoku.ac.jp*

Abstract: A novel direct path interference (DPI) suppression method is proposed in this paper for passive bistatic synthetic aperture radar (SAR) imaging applications. Conventional time-domain processing methods cannot mitigate the DPI completely and will introduce errors into the target position estimation. By exploiting the sparsity of the DPI signal and the properties of its covariance matrix, the proposed method solves these problems by accurately estimating the time delay of DPI based on the atomic minimization algorithm and Vandermonde decomposition in the frequency domain. The amplitude of DPI is then calculated by the least squares method. Simulations and experimental results of Wireless Fidelity (WiFi) based passive bistatic SAR imaging of short-range targets show that the proposed method can suppress DPI more effectively and estimate the position of the target more accurately than the classical method.

1 Introduction

Passive bistatic radar (PBR), which exploits existing illuminators of opportunity (IOs) instead of a dedicated radar transmitter, has received renewed interest for its large coverage capacity, low vulnerability, low cost, and reduced electromagnetic pollution to the environment [1, 2]. Various ground based and space based IOs, such as frequency-modulated broadcasting emitters, digital audio broadcasting (DAB) emitters, digital terrestrial television broadcasting (DTTB) emitters, global navigation satellite system (GNSS), and existing satellite synthetic aperture radar (SAR) systems, were employed for different applications [3–7]. Techniques of moving target detection and localization, high resolution SAR and inverse SAR imaging, and direction of arrival (DOA) estimation based on the PBR system have been proposed during the last decades [8–12].

For short range applications [13–16], such as tracking indoor human beings or man-made objects, through the wall target movement detection, and subsurface target mapping by ground penetrating radar (GPR) technique, a suitable IO should be exploited to satisfy the system requirement. Among different IOs, wireless local area network (LAN) may be a good choice for its wide bandwidth (40 / 80 MHz) and thus high range resolution (7.5 / 3.75 m in the air), its reasonable ambiguity function, its wide accessibility and coverage, and its wall/ground penetration capacity. As indicated in [17], IEEE 802.11 standards-based Wireless Fidelity (WiFi) signal is one of the most popular systems in wireless LAN that can be used for PBR applications. For WiFi based PBR, the ambiguity function analysis, range and Doppler frequency sidelobe reduction, high resolution SAR imaging by fusion of different IEEE 802.11ac WiFi signal bands, and cross-range resolution improvement by ISAR technique have been conducted in the last decade [18–20].

Since the transmitted signal from an existing IO is not within the control, a PBR system normally consists of two channels, the reference channel and the surveillance channel. The reference channel provides the time-delayed copies of the transmitted signal obtained by a directional reference antenna facing to the IO transmitter, while the surveillance channel records the echoes of the targets, which is obtained by a second antenna with broader radiation pattern, called as surveillance antenna, facing to the targets. Then, for moving target detection, a range-Doppler (RD) map is generated by calculating the 2D cross-ambiguity function between the reference channel and the surveillance channel based on the matched filtering approach. For stationary target imaging, the 1D cross-correlation is conducted at each antenna position for range compression, and then the back projection (BP) algorithm is used for the azimuth focusing [5, 10]. However, it is well known that the surveillance channel also contains the direct path interference (DPI) from the IO transmitter, which may be significantly stronger than the reflections of targets. Without suppressing the DPI, the targets are normally not detectable. Therefore, various methods have been proposed to confront this problem [21–25], including the CLEAN algorithm, least mean square (LMS) algorithm, fast and block LMS algorithm (FBLMS), extensive cancellation algorithm (ECA) and its variants, such as the batch based ECA (ECB) algorithm and the sequential cancellation batch (SCB) algorithm.

In the research of DPI suppression for PBR applications, it is found that the conventional time-domain based algorithms mentioned above may cause some problems when used in the short range applications. When the DPI is much stronger than the target reflections, the DPI cannot be completely mitigated since the time delay of DPI is not exactly integral times of the data sampling interval which forms the basis of these time-domain based algorithms. Therefore, the targets may still not be distinguished from the remaining components of DPI. When the targets become stronger, although these algorithms can suppress the DPI and make the targets clearer, the inaccurately estimated DPI components will introduce estimation errors of the target time delay, resulting in inaccurate target position estimation. To overcome this problem, we turn our attention to frequency-domain processing and propose a novel DPI suppression method based on the atomic norm minimization (ANM), Vandermonde decomposition, and LS method [26–29]. In the proposed method, we first estimate the time delay of the DPI and then estimate its amplitude in order to cancel it from the surveillance channel. The DPI time delay estimation problem is modelled as a

simple one-dimensional frequency estimation problem. By exploiting the sparsity of the DPI signal and the positive semidefinite (PSD), Toeplitz and low rank properties of its covariance matrix, the signal subspace of DPI is estimated by the ANM algorithm. Then, the Vandermonde decomposition is conducted and the DPI time delay is calculated by extracting the most significant frequency component from the surveillance signal. At last, the amplitude of the DPI component is estimated by the LS method. We have carried out several semi-experimental simulations and experiments of WiFi based passive bistatic SAR imaging to validate the proposed method. It is shown that the proposed method has better performance than the classical ECA method. The PDI can be effectively suppressed and the target position can be accurately estimated.

The rest of the paper is organized as follows. In Section 2, the signal model for PBR is established, and the classical DPI suppression methods are briefly introduced and their problems are discussed. In Section 3, the proposed DPI suppression method is presented and analysed, and the signal processing flowchart for WiFi based passive bistatic SAR imaging is also described. Simulation and experiment results are given in Section 4 to validate the performance of the proposed method. Finally, Section 5 concludes this paper and presents some considerations of the future work.

2 Passive radar signal model

As mentioned previously, a PBR system normally consists of a reference channel and a surveillance channel. The reference signal received by an antenna directly oriented to IOs (e.g., TV or WiFi transmitter) can be expressed as

$$s_{ref}(t) = A_{ref}s_0(t - t_{ref}) + n_{ref}(t) \tag{1}$$

where $s_0(t)$ is the transmitted signal, t denotes time, A_{ref} is the complex amplitude, t_{ref} denotes the time delay from the IO emitter to the reference antenna, and $n_{ref}(t)$ denotes the thermal noise.

Without considering the multipath echoes and moving targets, the received signal from a surveillance antenna, which includes the DPI, stationary target echoes, and thermal noise, can be expressed as (2), where A_{surv} is the amplitude of the DPI signal with time delay t_{surv}; P is the number of targets, a_p and t_p are the amplitude and time delay of the p-th target; and $n_{surv}(t)$ denotes the thermal noise in the surveillance channel.

In practice, the DPI is always much stronger than the target reflections, therefore needs to be suppressed to make the target detectable. Normally, time-domain processing methods, such as above mentioned ECA and LMS methods, are applied to this purpose. For these methods, the DPI signal is firstly estimated by the following equation with calculated coefficients $h(m)$ in the discrete form.

$$s_{dpi}(nT_s) = \sum_{m=0}^{M-1} h(m)s_{ref}\left[(n-m)T_s\right] \tag{3}$$

where T_s is the data sampling interval, $n = 0, 1, ..., N-1$ is the sample index, N is the number of samples, and M is the number of discrete time delays to properly model the maximum range of the DPI [21]. The differences among different time-domain DPI suppression algorithms are the methods used to estimate the coefficients $\boldsymbol{h}$. For example, in the ECA method, we have

$$\widetilde{\boldsymbol{h}} = (\boldsymbol{P}^H\boldsymbol{P})^{-1}\boldsymbol{P}^H\boldsymbol{s}_{surv} \tag{4}$$

where $\boldsymbol{P} \in C^{N\times M}$ is a matrix formed by the delayed copies of the reference signal vector $\boldsymbol{s}_{ref}$ (without considering the Doppler shifts of moving targets), $(\cdot)^H$ denotes the conjugate transpose operation, $(\cdot)^{-1}$ denotes the matrix inverse operation, and $\boldsymbol{s}_{surv}$ denotes the surveillance signal vector.

Then, the DPI suppressed surveillance signal can be obtained by

$$\widetilde{\boldsymbol{s}}_{surv} = \boldsymbol{s}_{surv} - \widetilde{\boldsymbol{s}}_{dpi} = \boldsymbol{s}_{surv} - \boldsymbol{P}\widetilde{\boldsymbol{h}} \tag{5}$$

At last, the time delay of the target can be estimated by calculating the cross-correlation function between the received reference signal and the DPI suppressed surveillance signal as

$$\chi(\tau) = \sum_{n=0}^{N-1} \widetilde{s}_{surv}(nT_s)s^*_{ref}(nT_s - \tau) \tag{6}$$

where τ is the expected time delay of the reflected signal from the target and $(\cdot)^*$ denotes complex conjugate.

However, since the time-domain DPI suppression algorithms are based on the data sampling interval T_s, as shown in (3), the DPI cannot be accurately estimated and completely suppressed because the delay of DPI, i.e. $\tau_{dpi} = t_{ref} - t_{surv}$, is not exactly integral times of T_s. Besides, by substituting (2) and (5) to (6), we can obtain

$$\begin{aligned}\chi(\tau) &= \sum_{n=0}^{N-1} \left(s_{surv}(nT_s) - \widetilde{s}_{dpi}(nT_s)\right) s^*_{ref}(nT_s - \tau) \\ &= \sum_{n=0}^{N-1} \left(s_{tar}(nT_s) + s^{error}_{dpi}(nT_s)\right) s^*_{ref}(nT_s - \tau)\end{aligned} \tag{7}$$

where $s^{error}_{dpi}(nT_s) = s_{dpi}(nT_s) - \widetilde{s}_{dpi}(nT_s)$ is the error produced by the inaccurate estimation of the DPI component, which will cause the inaccurate estimation of the time delay (i.e. range) of targets. Therefore, advanced algorithms are desired to accurately estimate the DPI component in the surveillance channel.

3 ANM based DPI suppression

In order to accurately estimate the DPI and then cancel it, we turn our attention to frequency domain signal processing. By Fourier transform, the frequency-domain reference signal and surveillance signal are given by (8) and (9).

$$s_{ref}(f) = A_{ref}s_0(f)e^{-j2\pi f t_{ref}} + n_{ref}(f) \tag{8}$$

where f denotes frequency .

Since the DPI is normally much stronger than the reflections of the targets, we can rewrite (9) as

$$\begin{aligned}s_{surv}(f) &= A_{surv}s_0(f)e^{-j2\pi f t_{surv}} + s_{\widetilde{n}}(f) \\ &= s_{dpi}(f) + s_{\widetilde{n}}(f)\end{aligned} \tag{10}$$

where $s_{\widetilde{n}}(f) = s_{tar}(f) + s_n(f)$ is assumed to be the additive noise to the main signal component $s_{dpi}(f)$.

Based on (8) and (10) and expressed in the discrete form, by using an inverse filter [30, 31], it can be derived that

$$s(f_n) = \begin{cases} A_0e^{j2\pi f_n\tau_{dpi}} + s_{noise}(f_n), & |s_{ref}(f_n)| \geq \delta \\ 0, & |s_{ref}(f_n)| < \delta \end{cases} \tag{11}$$

where $f_n = f_c + n\Delta f$ is the $(n+1)$-th frequency, f_c is the carrier frequency, Δf is the frequency step, $A_0 = A_{surv}/A_{ref}$, and δ is a user-defined threshold to avoid the numerical instability. We note that, (11) is obtained by $s(f_n) = s_{surv}(f_n)/s_{ref}(f_n)$. Compared to $s(f_n) = s_{surv}(f_n)s^*_{ref}(f_n)$, the division process can help to reduce the negative influences of the IO signal structures (i.e. the influence of $s_0(f)$) for range compression [30, 31]. However, in some cases, direct division is numerically unstable. Therefore, according to the amplitude of $s_{ref}(f_n)$, a user-defined threshold δ should be used to make $s(f_n) = 0$ if $|s_{ref}(f_n)| < \delta$ [31]. In this paper, we set $\delta = \sum_{n=0}^{N-1}|s_{ref}(f_n)|/4N$. Besides, in order to fairly show the advantages of the proposed method over conventional method, (6) is changed to

$$s_{surv}(t) = A_{surv}s_0(t - t_{surv}) + \sum_{p=1}^{P} a_p s_0(t - t_p) + n_{surv}(t) = s_{dpi}(t) + s_{tar}(t) + s_n(t) \tag{2}$$

$$s_{surv}(f) = A_{surv}s_0(f)e^{-j2\pi f t_{surv}} + \sum_{p=1}^{P} a_p s_0(f)e^{-j2\pi f t_p} + n_{surv}(f) = s_{dpi}(f) + s_{tar}(f) + s_n(f) \quad (9)$$

$$\chi(\tau) = \sum_{n=0}^{N-1} \widetilde{s}(f_n)e^{j2\pi f_n \tau} \quad (12)$$

where $\widetilde{s}(f_n) = \widetilde{s}_{surv}(f_n)/s_{ref}(f_n)$ if $|s_{ref}(f_n)| \geq \delta$ and $\widetilde{s}(f_n) = 0$ otherwise, and $\widetilde{s}_{surv}(f_n)$ is the $(n+1)$-th frequency component of the DPI suppressed surveillance signal.

By simple reformulations of (11), in case of $|s_{ref}(f_n)| \geq \delta$, we can obtain

$$\begin{aligned} s(f_n) &= A_0 e^{j2\pi f_c \tau} e^{j2\pi(n-1)\Delta f \tau_{dpi}} + s_{noise}(f_n) \\ &= \widetilde{A}_0 e^{j2\pi(n-1)\Delta f \tau_{dpi}} + s_{noise}(f_n) \\ &= s_0(f_n) + s_{noise}(f_n) \end{aligned} \quad (13)$$

and, in the vector form, we have the following $N_1 \times 1$ signal vector

$$\boldsymbol{s} = \boldsymbol{\Phi}\boldsymbol{s}_0 + \boldsymbol{s}_{noise} \quad (14)$$

where $\boldsymbol{\Phi}$ is the measurement matrix with size $N_1 \times N$ that used to sample $\boldsymbol{s}_0$ according to the criterion $|s_{ref}(f_n)| \geq \delta$, $N_1 \leq N$ is the number of frequencies that satisfy this criterion, $\boldsymbol{s}_0 = \widetilde{A}_0 \boldsymbol{s}_{steer}$ is a $N \times 1$ vector,

$$\boldsymbol{s}_{steer} = [1, e^{j2\pi f_{dpi}}, ..., e^{j2\pi(N-1)f_{dpi}}]^T \quad (15)$$

is the steering vector corresponding to f_{dpi}, $[\cdot]^T$ denotes the transpose operation, and $f_{dpi} = \Delta f \tau_{dpi}$.

It can be learned from (14) that the DPI time delay estimation problem is a one-dimensional frequency estimation problem of the sinusoidal signal $\boldsymbol{s}_0$ with time samples $(0, 1, ..., N-1)$ and frequency f_{dpi}. Recently, based on the intrinsic sparsity of DPI, sparse representation (SR) and compressive sensing (CS) based methods have been proposed to estimate the frequency of $\boldsymbol{s}_0$ from its noise polluted under-sampled signal $\boldsymbol{s}$ by solving the following minimization problem.

$$\widetilde{\boldsymbol{\alpha}} = \min |\boldsymbol{\alpha}|_0 \quad s.t. ||\boldsymbol{s} - \boldsymbol{\Phi}\boldsymbol{\Theta}\boldsymbol{\alpha}||_2^2 \leq \varepsilon_n \quad (16)$$

where

$$\boldsymbol{\Theta} = [e^{j2\pi\Delta \boldsymbol{f}\tau_1}, e^{j2\pi\Delta \boldsymbol{f}\tau_2}, ..., e^{j2\pi\Delta \boldsymbol{f}\tau_L}] \in C^{N\times L} \quad (17)$$

$\Delta \boldsymbol{f} = [0, 1, ..., N-1]^T \Delta f$, $\boldsymbol{\alpha}$ is the coefficient vector corresponding to the time delay $[\tau_1, \tau_2, ..., \tau_L]$, and ε_n denotes the noise level (containing weak targets and thermal noise).

Although (16) is a non-deterministic polynomial-time hard (NP-hard) problem, a number of computationally efficient algorithms can be used, such as the smooth L0 (SL0) algorithm and orthogonal matching pursuit (OMP) algorithm [32, 33]. However, for these conventional SR/CS based algorithms, as formulated by (16), the expected frequencies are assumed to be located at fix discretised grids $[\Delta f\tau_1, \Delta f\tau_2, ..., \Delta f\tau_L]$. The off-grid problem, i.e the mismatch between the pre-defined frequency grid and the actual frequency of signal, may cause the performance degradation [34, 35].

It is known that the covariance matrix of $\boldsymbol{s}_0$, i.e.

$$\boldsymbol{R}_0 = E[\boldsymbol{s}_0\boldsymbol{s}_0^H] = E\left(|\widetilde{A}_0|^2\right)\boldsymbol{s}_{steer}\boldsymbol{s}_{steer}^H \quad (18)$$

is a rank-1 PSD block-Toeplitz matrix with size $N \times N$, where $E[\cdot]$ denotes the expectation. Therefore, by exploiting these structures, the frequencies of $\boldsymbol{s}_0$ can be exactly retrieved from its covariance matrix $\boldsymbol{R}_0$ by the classical Vandermonde decomposition, with which as the basis some subspace based methods, such as MUSIC and ESPRIT, have been proposed to estimate the frequency of $\boldsymbol{s}_0$. However, for these methods, a sufficient number of training samples is required to estimate the signal subspace. In this paper, the ANM algorithm, which directly deals with the continuous frequencies and completely resolves the off-grid problem of SR/CS based methods without the requirement of training samples as other subspace based methods, is applied to estimate $\boldsymbol{s}_0$ and its subspace.

We know that, rather than in the discretised frequency domain, $\boldsymbol{s}_0$ is sparse in the continuous frequency domain. We can further learn from (14) that $\boldsymbol{s}_0$ can be formed by an atom in the atomic set

$$\mathscr{A} \triangleq \{\boldsymbol{s}_{steer}(\boldsymbol{f})|\boldsymbol{f} \in [0, 1)\} \quad (19)$$

that collects all the potential steering vectors $\boldsymbol{s}_{steer}$. Thus, with the atomic L0 norm of $\boldsymbol{s}_0$ defined as

$$||\boldsymbol{s}_0||_{\mathscr{A},0} \triangleq \inf_{\alpha_o \in C, \boldsymbol{f}_o \in [0,1)} \left\{ O|\boldsymbol{s}_0 = \sum_{o=1}^{O} \alpha_o \boldsymbol{s}_{steer}^o(\boldsymbol{f}_o) \right\} \quad (20)$$

to exploit the sparsity of $\boldsymbol{s}_0$, where O is the number of atoms in $\mathscr{A}$ that represent $\boldsymbol{s}_0$, the DPI component can be extracted from $\boldsymbol{s}$ by the following ANM problem.

$$\widetilde{\boldsymbol{s}}_0 = \min ||\boldsymbol{s}_0||_{\mathscr{A},0}, \quad s.t. ||\boldsymbol{s} - \boldsymbol{\Phi}\boldsymbol{s}_0||_2^2 \leq \varepsilon_n \quad (21)$$

Furthermore, because $||\boldsymbol{s}_0||_{\mathscr{A},0} = \text{rank}(\boldsymbol{R}_0) = 1$, it can also be derived that (21) equals the following problem [27].

$$\begin{aligned} [\widetilde{\boldsymbol{s}}_0, \widetilde{\boldsymbol{R}}_0] &= \min_{\boldsymbol{R}_0, \boldsymbol{s}_0} \text{rank}(\boldsymbol{R}_0) \\ s.t. &\begin{bmatrix} 1 & \boldsymbol{s}_0^H \\ \boldsymbol{s}_0 & \boldsymbol{R}_0 \end{bmatrix} \geq 0, ||\boldsymbol{s} - \boldsymbol{\Phi}\boldsymbol{s}_0||_2^2 \leq \varepsilon_n \end{aligned} \quad (22)$$

where $\text{rank}(\cdot)$ denotes the rank of a matrix.

The rank minimization problem in (22) is also NP-hard as (16), therefore more computationally efficient methods should be adopted. Besides, although it is expected that $\widetilde{\boldsymbol{R}}_0$ in (22) is the estimation of the covariance matrix of $\boldsymbol{s}_0$, it is shown that $\widetilde{\boldsymbol{R}}_0$ is only the estimation of the subspace of $\boldsymbol{s}_0$. Therefore, the following nuclear norm relaxation of (22) [28] is used to estimate $\boldsymbol{s}_0$ and its subspace $T(\boldsymbol{u})$, i.e. a Toeplitz matrix formed by a vector $\boldsymbol{u}$.

$$\begin{aligned} [\widetilde{\boldsymbol{s}}_0, \widetilde{\boldsymbol{u}}] &= \min_{\boldsymbol{s}_0, \boldsymbol{u}} \text{trace}[T(\boldsymbol{u})] \\ s.t. &\begin{bmatrix} 1 & \boldsymbol{s}_0^H \\ \boldsymbol{s}_0 & T(\boldsymbol{u}) \end{bmatrix} \geq 0, ||\boldsymbol{s} - \boldsymbol{\Phi}\boldsymbol{s}_0||_2^2 \leq \varepsilon_n \end{aligned} \quad (23)$$

where $\text{trace}[\cdot]$ denotes the trace of a matrix.

In this paper, (23) is solved by the SDP solver in CVX. Then, since DPI is the strongest component in $\boldsymbol{s}$, instead of $\boldsymbol{s}_{tar} + \boldsymbol{s}_n = \boldsymbol{s} - \boldsymbol{\Phi}\widetilde{\boldsymbol{s}}_0$ after obtaining the estimation of $\boldsymbol{s}_0$, which may also suppress the target components, we propose to use the following method to achieve the DPI suppressed pure signal.

$$\boldsymbol{s}_{pure} = \boldsymbol{s}_{tar} + \boldsymbol{s}_n = \boldsymbol{s} - \beta\boldsymbol{\Phi}\widetilde{\boldsymbol{s}}_{steer}^1 \quad (24)$$

where

$$\widetilde{\boldsymbol{s}}_{steer}^1 = [1, e^{j2\pi f_\tau^1}, ..., e^{j2\pi(N-1)f_\tau^1}]^T \quad (25)$$

is the estimation of the steering vector of DPI,

$$\beta = [(\boldsymbol{\Phi}\widetilde{\boldsymbol{s}}_{steer}^1)^H \boldsymbol{\Phi}\widetilde{\boldsymbol{s}}_{steer}^1]^{-1} (\boldsymbol{\Phi}\widetilde{\boldsymbol{s}}_{steer}^1)^H \boldsymbol{s} \quad (26)$$

is the amplitude of the DPI estimated by least square method, $f_\tau^1 = \Delta f \tau^1$ is the most significant frequency of $\boldsymbol{s}_0$ estimated by the Vandermonde decomposition of $T(\boldsymbol{u})$, i.e.

$$T(\boldsymbol{u}) = \sum_{k=1}^{K} p_k \widetilde{\boldsymbol{s}}_{steer}^{k} (\widetilde{\boldsymbol{s}}_{steer}^{k})^H = \boldsymbol{A}\boldsymbol{P}\boldsymbol{A}^H \quad (27)$$

and τ^1 is the time delay estimation of the DPI.

At last, the inverse Fourier transform can be carried out to estimate the time delays of targets, giving

$$\chi_{anm}(\boldsymbol{\tau}) = \sum_{n_1=0}^{N_1-1} s_{pure}(f_{n_1}) e^{j2\pi f_{n_1}\boldsymbol{\tau}} \quad (28)$$

where f_{n_1} is the (n_1+1)-th frequency that satisfy the criterion $|s_{ref}(f_{n_1})| \geq \delta$.

We should note that, for moving target detection by PBR, beyond the DPI suppression, the strong echoes of the ground stationary targets should also be mitigated from the surveillance channel. Since we are focusing on the passive bistatic SAR imaging applications, all the stationary targets should be imaged. Therefore, in the established signal model and the derivation of the proposed method, $\boldsymbol{s}_{dpi}$ is assumed to only contain one strong signal, thus $\boldsymbol{s}_0$ only has one significant frequency and the rank of the signal covariance matrix equals to 1, i.e. $\mathrm{rank}(\boldsymbol{R}_0) = 1$. However, the proposed method can be easily extended to the multiple components suppression problem, such as the moving target range-Doppler mapping, or the reduction of strong multiple echoes, or the specific SAR imaging case where the strong stationary targets make the weak stationary targets undetectable and thus a CLEAN-like approach is desired to apply. In such a case, the DPI component should be changed to

$$s_{dpi}(t) = \sum_{i=1}^{I} A_{surv}^{i} s_0(t - t_{surv}^{i}) \quad (29)$$

and

$$\boldsymbol{s}_0 = \sum_{i=1}^{I} \widetilde{A}_0^i \boldsymbol{s}_{steer}^i \quad (30)$$

where I is the number of unwanted components in the surveillance channel. As the consequence, (23) and (24) should be modified to

$$\begin{aligned} &[\widetilde{\boldsymbol{s}}_0, \widetilde{\boldsymbol{u}}] = \min_{\boldsymbol{s}_0, \boldsymbol{u}} \mathrm{trace}[T(\boldsymbol{u})] \\ &s.t. \begin{bmatrix} I & \boldsymbol{s}_0^H \\ \boldsymbol{s}_0 & T(\boldsymbol{u}) \end{bmatrix} \geq 0, ||\boldsymbol{s} - \boldsymbol{\Phi}\boldsymbol{s}_0||_2^2 \leq \varepsilon_n \end{aligned} \quad (31)$$

and

$$\boldsymbol{s}_{pure} = \boldsymbol{s}_{tar} + \boldsymbol{s}_n = \boldsymbol{s} - \boldsymbol{\Phi}\boldsymbol{\Psi}\boldsymbol{\beta} \quad (32)$$

where

$$\boldsymbol{\Psi} = [\widetilde{\boldsymbol{s}}_{steer}^1, \widetilde{\boldsymbol{s}}_{steer}^2, ..., \widetilde{\boldsymbol{s}}_{steer}^I] \quad (33)$$

and

$$\boldsymbol{\beta} = [(\boldsymbol{\Phi}\boldsymbol{\Psi})^H (\boldsymbol{\Phi}\boldsymbol{\Psi})]^{-1} (\boldsymbol{\Phi}\boldsymbol{\Psi})^H \boldsymbol{s} \quad (34)$$

Since we are focusing on the short range passive bistatic SAR imaging with WiFi signals, the signal processing procedure based on the proposed DPI suppression method for target imaging is also presented. In a passive SAR system, in order to achieve a high azimuth resolution, the surveillance antenna is moved linearly to form a synthetic aperture. When the surveillance antenna is at the l-th position $(x_l, 0)$, the proposed DPI suppression method can be used and the l-th range-compressed profile can be obtained by (28) as

$$\chi_{anm}^{l}(\boldsymbol{\tau}) = \sum_{n_1=0}^{N_1-1} s_{pure}^{l}(f_{n_1}) e^{j2\pi f_{n_1}\boldsymbol{\tau}} \quad (35)$$

where $l = 1, 2, ..., L$ and $\boldsymbol{s}_{pure}^{l}$ is the l-th DPI suppressed frequency signal. Then, by using the BP algorithm, the reflection coefficient of the target at (x, y) can be estimated by

$$\widetilde{\sigma}(x,y) = \sum_{l=1}^{L} \chi_{anm}^{l}[t_{ref} - \tau_l(x,y)] \quad (36)$$

where $\tau_l(x,y) = [r_l(x,y) + r_0(x,y)]/c$, c is the velocity of light , $r_0(x,y) = \sqrt{(x_0 - x)^2 + (y_0 - y)^2}$ is the distance between the target and the IO emitter, i.e. the WiFi access point (AP) in our case, at (x_0, y_0), $r_l(x,y) = \sqrt{(x_l - x)^2 + y^2}$, and $\widetilde{\sigma}(x,y)$ is the estimated amplitude of the target at (x, y). During the coherent summation of the range-compressed signal from all the antenna positions, many high-level artifacts will be produced by BP algorithm. It has been shown in [36] that the cross-correlation based BP (called as CC-BP in this paper) algorithm can effectively suppress the artifacts. Therefore, in this paper, the CC-BP algorithm is applied to estimate the reflection coefficients of targets, which can be expressed as

$$\begin{aligned} \widetilde{\sigma}(x,y) = \sum_{l_1=1}^{L-1} \sum_{l_2=l_1+1}^{L} \{&\chi_{anm}^{l_1}[t_{ref} - \tau_{l_1}(x,y)] \\ &\times \chi_{anm}^{l_2}[t_{ref} - \tau_{l_2}(x,y)]\} \end{aligned} \quad (37)$$

In summary, the signal processing chain for passive bistatic SAR imaging is presented in Fig. 1.

4 Simulation and experiment results

In this section, we present some simulation and experiment results to demonstrate the effectiveness of the proposed DPI suppression method and the performance of the presented short range passive bistatic SAR imaging scheme. The classical ECA algorithm with different number of discrete time delays (range cells) that models the maximum range of the DPI, i.e. different value of M, is used for the comparison.

4.1 Semi-experimental simulation results

In the first study step, we did some semi-experimental simulations, where the reference signal is obtained by directly sampling the IEEE 802.11n 2.422 GHz signal with 40 MHz bandwidth from a WiFi AP using a horn antenna, while the surveillance signal at each antenna position is simulated with time delays corresponding to the assumed target position. The synthetic aperture length is set to 3 m with a step of 5 cm from (-1.5, 0) to (1.5, 0), the reference antenna and the AP are assumed to be located at (0, 0), and the data sampling frequency is 10 GSamples/s (0.1 ns data sampling interval and thus 0.03 m long for each range cell) to avoid the signal aliasing. We simulate the DPI with random time delay for each antenna position, and the amplitude of DPI is 100 times (40 dB) stronger than the target. The minimal DPI delay corresponds to about 50 range cells and the maximal one is about 100 range cells.

For the first simulation, only one target at (0, 5) is simulated. Before DPI suppression, the range compressed profiles for different surveillance antenna positions and the imaging result by CC-BP algorithm are shown in Fig. 2. It can be observed that, since the DPI is much stronger than the target echo, the target cannot be distinguished.

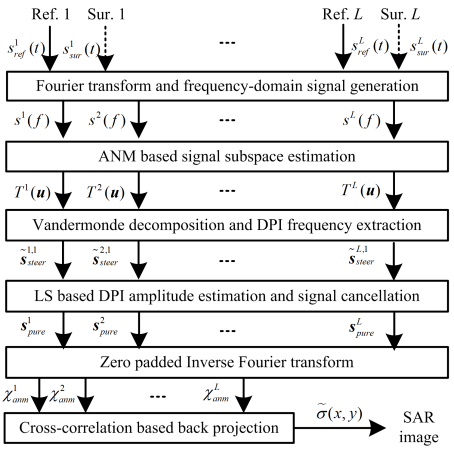

Fig. 1: Signal processing chain for passive bistatic SAR imaging

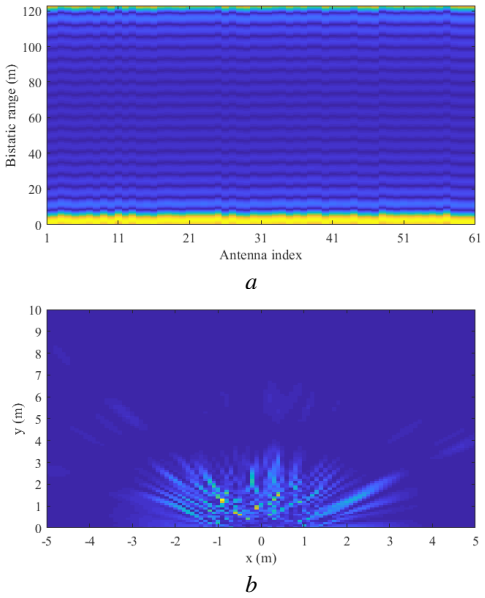

Fig. 2: Results for one target before strong DPI suppression
a Range profiles
b Focused SAR image

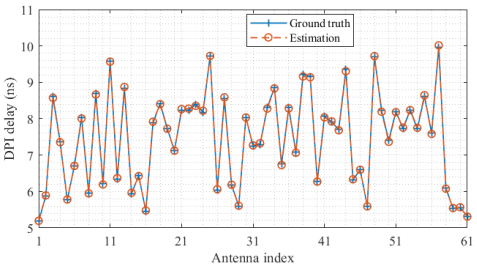

Fig. 3: DPI time delay estimation via the proposed method

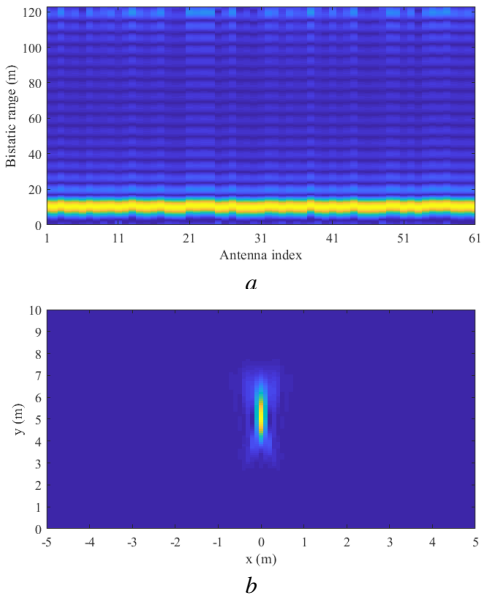

Fig. 4: Results for one target after strong DPI suppression via the proposed method
a Range profiles
b Focused SAR image

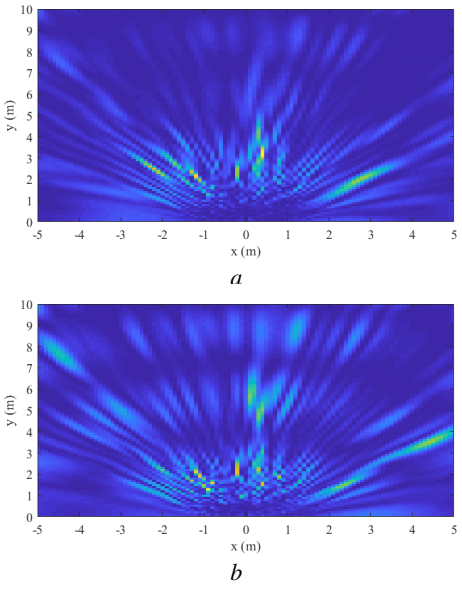

Fig. 5: Focused images of one target after strong DPI suppression via the ECA method with different range cells
a 51 range cell
b 101 range cells

As to the proposed DPI suppression based method, the time delay of DPI for each antenna position is estimated accurately, as shown in Fig. 3. Therefore, with further processing by Vandermonde decomposition and LS method, the DPI can be effectively suppressed, the target can be clearly seen and its estimated position is also accurate, as shown in Fig. 4. For the ECA method, different range cells are considered (i.e. 51 and 101 range cells, which are decided by the minimal and maximal DPI delays). Since the delays of DPI are randomly simulated and are not integral times of the sampling interval (0.1 ns), the strong DPI cannot be effectively suppressed by the ECA technique, and the target is still undistinguished, as shown in Fig. 5.

Then, three targets at (0, 5), (-2.5, 5), and (2.5, 5) are simultaneously simulated. The imaging results obtained after DPI suppression by the ECA method with 101 range cells and the proposed method

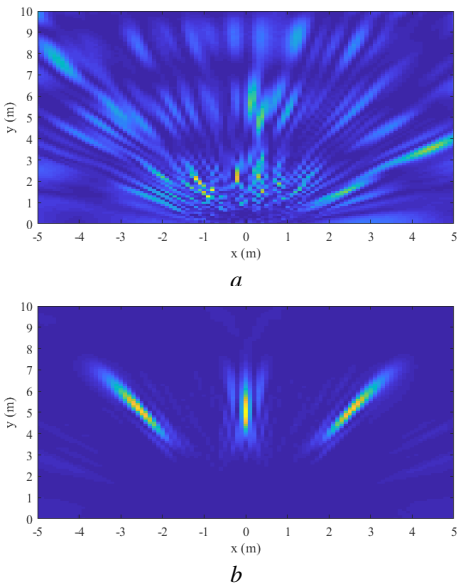

Fig. 6: Focused images of three targets after strong DPI suppression via different methods
a ECA method with 101 range cell
b The proposed method

are shown in Fig. 6. The advantage of the proposed method over the ECA method is unchanged for the multiple targets case.

In the second study step, we change the strength of the DPI. Although we still consider random DPI time delay at each surveillance antenna position, the amplitude of the simulated DPI is changed to 5 times (14 dB) stronger than the target. In such a case, for the proposed ANM based signal subspace estimation approach, the signal to noise ratio (SNR) is decreased, which is used to mimic a much more noisy condition than the previous simulations.

The imaging result obtained by CC-BP algorithm before DPI suppression, DPI time delay estimation result, range compressed profiles, and focused image obtained after the DPI suppression by the proposed method are shown in Fig. 7. It can be learned from Fig. 7 (a) that, before DPI suppression, the target is already detectable but not clear enough, therefore DPI suppression is still necessary. Compared with Fig. 3, Fig. 7 (b) demonstrates that, in the more noisy condition (26 dB), the performance of the proposed method will be degraded. However, the time delay of DPI can still be estimated for each surveillance antenna position. Therefore, as shown in Fig. 7 (c) and Fig. 7 (d), the DPI can be mitigated effectively and the target is much clearer than Fig. 7 (a).

The range profiles and focused images obtained after DPI suppression via ECA method with 51 range cells (minimal DPI delay) and 101 range cells (maximal DPI delay) are shown in Fig. 8 (a) and (b), respectively. Different from the strong DPI case as shown in Fig. 5, for weaker DPI, the ECA method with 51 range cells and 101 range cells can work well. Since most energy of the DPI can be suppressed, a smaller DPI energy than the target can be obtained, making the target clearer. However, compared with the proposed method, there are some random artifacts in the focused SAR images. Furthermore, the inaccurate estimation of the DPI component will cause the inaccurate estimation of the target position, i.e. the target will be shifted in the focused SAR images, as shown in Fig. 9. It can be observed that, because of DPI estimation error, the ECA method will give incorrect target position estimation, especially in the y direction, which is actually 5 m. Compared with 51 range cells, the ECA method with 101 range cells shows a even worse result.

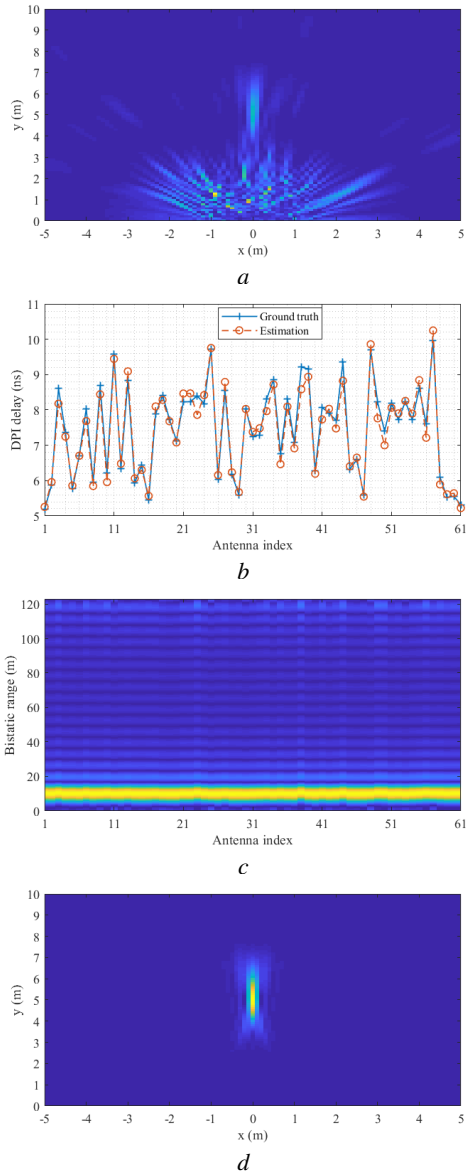

Fig. 7: Proposed method applied to one target case with weaker DPI
a Focused image before DPI suppression
b DPI time delay estimation
c Range profiles after DPI suppression
d Focused image after DPI suppression

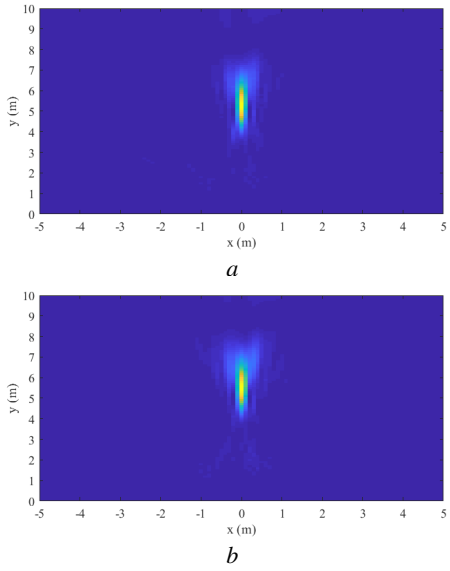

Fig. 8: ECA method applied to one target case with weaker DPI
b Focused image after DPI suppression with 51 range cell
d Focused image after DPI suppression with 101 range cells

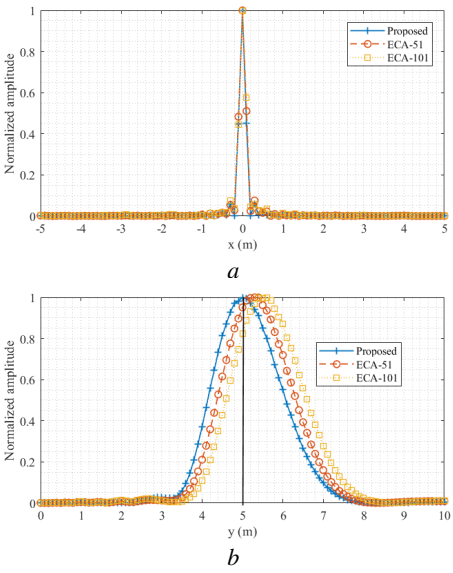

Fig. 9: Simulated target position estimation accuracy comparison
a x-direction
b y-direction

4.2 *Experiment results*

Experiments are also conducted to validate the proposed DPI suppression method. The experiment setup is shown in Fig. 10, where a metallic plate located at about (-0.5, 6) is set to be the imaging target. The WiFi AP is at (-1.5, 1), the reference antenna is at (-1.5, 2), and the surveillance antenna is sledded on a rail from (-1.5, 0) to (1.5, 0) with a step of 5 cm.

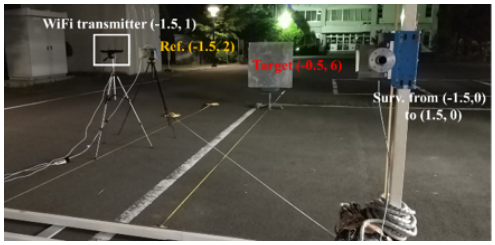

Fig. 10: Experiment setup for WiFi based passive bistatic SAR imaging for short-range target

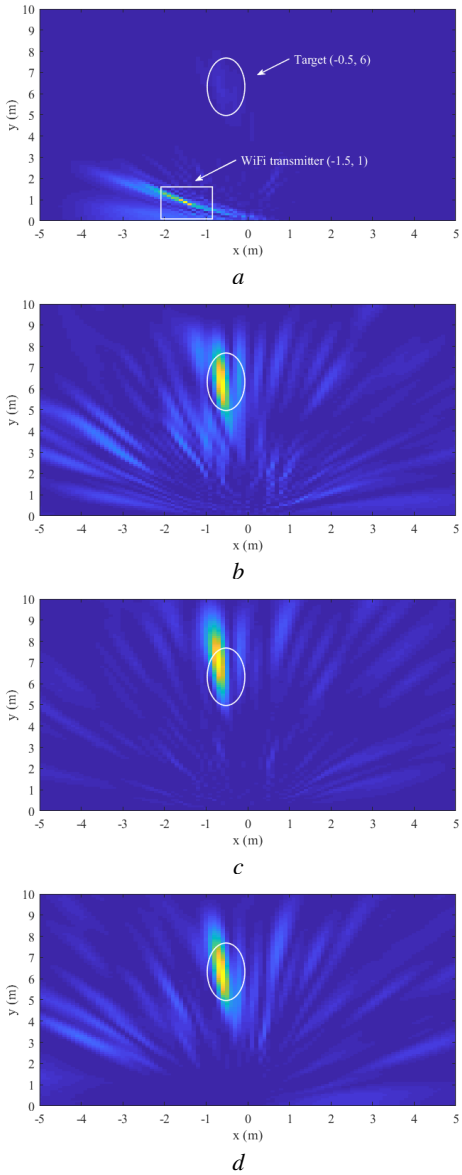

a

b

c

d

Fig. 11: Focused images of the metallic plate at about (-0.5, 6)
a Before DPI suppression
b After DPI suppression via ECA method with 21 range cell
c After DPI suppression via ECA method with 121 range cells
d After DPI suppression via the proposed method

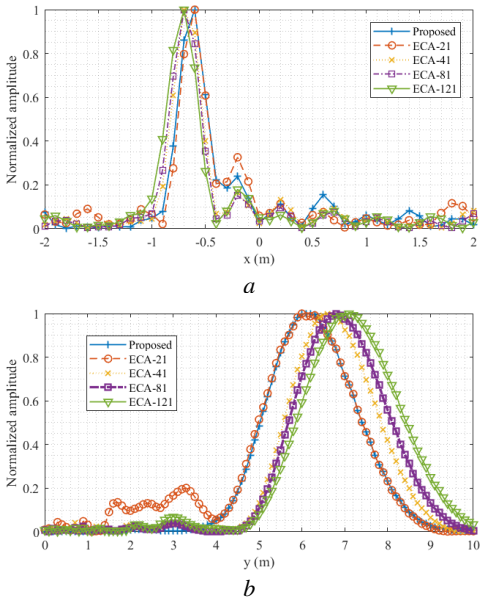

a

b

Fig. 12: Real target position estimation accuracy comparison
a x-direction
b y-direction

The imaging result without DPI suppression is shown in Fig. 11 (a). Since the DPI is stronger than the reflection of the metallic plate in this experiment, the target cannot be well observed from the focused image. Besides, because the position of WiFi AP is unchanged for each surveillance antenna position, the DPI time delay is not randomly distributed as in the simulation case, but follows a hyperbolic function of the antenna position. Therefore, the WiFi AP can be focused by the CC-BP algorithm with accurate position (-1.5, 1), as indicated by the white rectangle in Fig. 11 (a). Moreover, based on the experiment setup, the minimal DPI delay corresponds to 33.3 range cells and the maximal one is about 105.4 rang cells, which can be the reference value for range cell number selections for ECA method.

Firstly, with 21 range cell, the DPI can be suppressed by the ECA method to some extents, as shown in Fig. 11 (b). However, due to the residual of the DPI component, there are many artifacts in the focused image. Because of some errors introduced by the inaccurately estimated DPI component, with 121 range cells, ECA method can further suppress the DPI but with the cost of the degraded accuracy of target position, as shown in Fig. 11 (c) and indicated by the white circle. For the proposed method, even though the DPI is not significantly dominant in the received surveillance channel, its influence can still be effectively suppressed, as shown in Fig. 11 (d), where the target is clearly distinguished from the background and the position of the target is not influenced by the suppression of DPI.

Then, we present the target position estimation accuracy comparison between the proposed method and the ECA method with different number of rang cells. Two cross-sections along the x-direction and y-direction of the focused images obtained by different methods are shown in Fig. 12. It can be learned that, with the increase of the processing range cells, the target will be further shifted by the ECA method. The proposed method can provide more accurate estimation of the target position. Moreover, although the ECA method with 21 range cells can obtain the similar target position estimation accuracy with the proposed method, its artifact level is higher than the proposed method.

At last, the computational complexity of the proposed method is discussed. For the proposed method, solving (23) is the most time consuming step, compared to which the computing time of other steps can be ignored. In our study, (23) is solved by the SDP

solver SDPT3 implemented in CVX, where the semi-definite constraint is of size $N \times N$. As indicated in [37], the SDP step has the computational complexity of $\mathrm{O}(N^{4.5})$. For the ECA method, the computational complexity is about $\mathrm{O}(NM^2 + M^3)$ [22]. In the simulation and experiment, the data sampling frequency is 10 GSamples/s and the number of samples is N=4096, which implies the proposed method is much more time consuming. However, we note that, since not all the sampled signal that within 10 GHz bandwidth is useful for the passive bistatic SAR imaging, but only the WiFi signal is needed to extract for processing. Therefore, in the implementation of the proposed method, only the frequencies within the 40 MHz WiFi bandwidth around the 2.422 GHz central frequency were processed. In other words, in the proposed method, the value of N can be much reduced.

Therefore, measured by the TIC and TOC instruction in MATLAB, averaged by 100 Monte-Carlo trials, and implemented in MATLAB 2015b on a Core i5, 2.5GHz, 8GB RAM PC, the computing time of the proposed method and the ECA method with 100 rang cell, 200 range cells and 400 range cells (corresponding to the maximal DPI distance of 3 m, 6 m and 12 m) for passive SAR imaging are 40.17 seconds, 6.95 seconds, 15.73 seconds, 45.48 seconds, respectively. This indicates that the proposed method is more time consuming than the ECA method with a small number of processing range cells, but is comparable with the ECA method with a large number of processing range cells.

5 Conclusion

In this paper, we have proposed and validated an effective direct path interference (DPI) suppression method for passive bistatic radar applications. By employing the advanced atomic norm minimization algorithm and the classical Vandermonde decomposition algorithm, we can estimate the time delay of DPI accurately, and thus the influence of DPI on the short range target imaging can be reduced by the least squares method. Compared to the classical time-domain DPI suppression method, the proposed method demonstrates the advantages in terms of DPI suppression capacity and target position estimation accuracy. We have carried out several semi-experiment simulations and experiments of WiFi based passive SAR imaging to demonstrate the effectiveness of the proposed method. When the DPI component is not significantly stronger than the echoes of targets in the surveillance channel, i.e. with the noisy conditions, the proposed method can still work well. Furthermore, we also presented the potential implementations of the proposed method for moving target range-Doppler mapping and strong stationary target removal in some specific passive SAR applications. The computational complexity of the proposed method is comparable with the conventional ECA method with large number of range cells, but needs to be further reduced. In practice, the sparsity of the DPI and the low rank property of its covariance matrix may be destroyed by some practical factors. Therefore, our next study step is to further improve the performance of the proposed method in practical environments, and to reduce its computing time to realize real-time processing.

6 Acknowledgments

This work was supported by JSPS Grant-in-Aid for Scientific Research (A) 26249058, OscillatorIMP and FIRST-TP grants from the French Projet d'Investissement d'Avenir (PIA), as well as Tohoku University through the funding of an invited scientist position for J.-M Friedt and a ROIS scholarship for Zhipeng Hu.

7 References

1 Palmer, J., Palumbo, S., Summers, A., Merrett, D., Searle, S., Howard, S.:'An overview of an illuminator of opportunity passive radar research project and its signal processing research directions', *Digital Signal Processing*, 2011, **21** (5), pp.593–599

2 Capria, A., Giusti, E., Moscardini, C., Conti, M., Petri, D., Martorella, M., Berizzi, F.:'Multifunction imaging passive radar for harbour protection and navigation safety', *IEEE Aerospace and Electronic Systems Magazine*, 2017, **32** (2), pp.30–38

3 Howland, P. E., Maksimiuk, D., Reitsma, G.:'FM radio based bistatic radar', *IEE Proceedings-Radar, Sonar and Navigation*, 2005, **152** (3), pp.107–115

4 Coleman, C., Yardley, H.:'Passive bistatic radar based on target illuminations by digital audio broadcasting', *IET Radar, Sonar and Navigation*, 2008, **2** (5), pp.366–375

5 Feng, W., Friedt, J. M., Cherniak, G., Sato, M.:'Novel algorithm for high resolution passive radar imaging with ISDB-T digital TV signal', Proc. IEEE Int. Geosci. Remote Sens. Symp., Valencia, Spain, July 2018, pp. 1–4

6 Zeng, T., Zhang, T., Tian, W., Hu, C.:'A novel subsidence monitoring technique based on space-surface bistatic differential interferometry using GNSS as transmitters', *Science China Information Sciences*, 2015, **58** (6), pp.1–16

7 Zhang, H., Deng, Y., Wang, R., Li, N., Zhao, S., Hong, F., Wu, L., Loffeld, O.:'Spaceborne/stationary bistatic SAR imaging with TerraSAR-X as an illuminator in staring-spotlight mode', *IEEE Transactions on Geoscience and Remote Sensing*, 2016, **54** (9), pp.5203–5216

8 Falcone, P., Colone, F., Macera, A., Lombardo, P.:'Two-dimensional location of moving targets within local areas using WiFi-based multistatic passive radar', *IET Radar, Sonar and Navigation*, 2014, **8** (2), pp.123–131

9 Wu, Q., Zhang, Y.D., Amin, M.G., Himed, B.:'Space–time adaptive processing and motion parameter estimation in multistatic passive radar using sparse Bayesian learning', *IEEE Transactions on Geoscience and Remote Sensing*, 2016, **54** (2), pp.944–957

10 Gromek, D., Kulpa, K., Samczyński, P.:'Experimental results of passive SAR imaging using DVB-T illuminators of opportunity', *IEEE Geoscience and Remote Sensing Letters*, 2016, **13** (8), pp.1124–1128

11 Qiu, W., Giusti, E., Bacci, A., Martorella, M., Berizzi, F., Zhao, H., Fu, Q.:'Compressive sensing–based algorithm for passive bistatic ISAR with DVB-T signals', *IEEE Transactions on Aerospace and Electronic Systems*, 2015, **51** (3), pp.2166–2180

12 Wang, J., Wang, H.T., Zhao, Y.:' Direction finding in frequency-modulated-based passive bistatic radar with a four-element adcock antenna array', *IET radar, sonar and navigation*, 2011, **5** (8), pp.807–813

13 Chetty, K., Smith, G.E.,Woodbridge, K.:'Through-the-wall sensing of personnel using passive bistatic wifi radar at standoff distances', *IEEE Transactions on Geoscience and Remote Sensing*, 2012, **50** (4), pp.1218–1226

14 Huang, D., Nandakumar, R., Gollakota, S.:'Feasibility and limits of wi-fi imaging', Proc. ACM Conf. Embedded Netw. Sensor Syst., ACM, November 2014, pp. 266–279

15 Feng, W., Friedt, J-M., Goavec-Merou, G., Sato M.:'Passive radar delay and angle of arrival measurements of multiple acoustic delay lines used as passive sensors', *IEEE Sensors Journal*, 2018, in press

16 Feng, W., Friedt, J-M., Hu, Z., Sato M.:' WiFi-based imaging for ground penetrating radar applications: fundamental research and experimental results', IET International Radar Conference, Nanjing, China, Oct. 2018

17 Colone, F., Falcone, P., Bongioanni, C., Lombardo, P.:'WiFi-based passive bistatic radar: Data processing schemes and experimental results', *IEEE Transactions on Aerospace and Electronic Systems*, 2012, **48** (2), pp.1061–1079

18 Colone, F., Woodbridge, K., Guo, H., Mason, D., Baker, C.J.:'Ambiguity function analysis of wireless LAN transmissions for passive radar', *IEEE Transactions on Aerospace and Electronic Systems*, 2011, **47** (1), pp.240–264

19 Shi, J., Liu, Y., Liu, W., Zhang, X.:'High-resolution synthetic aperture radar based on the IEEE 802.11 protocol', *Electronics Letters*, 2015, **51** (22), pp.1815–1817

20 Colone, F., Pastina, D., Falcone, P., Lombardo, P.:'WiFi-based passive ISAR for high-resolution cross-range profiling of moving targets', *IEEE Transactions on Geoscience and Remote Sensing*, 2014, **52** (6), pp.3486–3501

21 Garry, J.L., Baker, C.J., Smith, G.E.:'Evaluation of direct signal suppression for passive radar', *IEEE Transactions on Geoscience and Remote Sensing*, 2017, **55** (7), pp.3786–3799

22 Ansari, F., Taban, M.R., Gazor, S.:'A novel sequential algorithm for clutter and direct signal cancellation in passive bistatic radars', *EURASIP Journal on Advances in Signal Processing*, 2016, **1**, p.134

23 Colone, F., O'hagan, D.W., Lombardo, P., Baker, C.J.:'A multistage processing algorithm for disturbance removal and target detection in passive bistatic radar', *IEEE Transactions on Aerospace and Electronic Systems*, 2009, **45** (2), pp. 698–722

24 Cardinali, R., Colone, F., Ferretti, C., Lombardo, P.:'Comparison of clutter and multipath cancellation techniques for passive radar', Proc. IEEE Radar Conf., April 2007, pp. 469–474

25 Palmer, J.E., Searle, S.J.:'Evaluation of adaptive filter algorithms for clutter cancellation in passive bistatic radar', Proc. IEEE Radar Conf., May 2012, pp. 493–498

26 Tang, G., Bhaskar, B.N., Shah, P., Recht, B.:'Compressed sensing off the grid', *IEEE transactions on information theory*, 2013, **59** (11), pp.7465–7490

27 Yang, Z., Xie, L.:'Exact joint sparse frequency recovery via optimization methods', *IEEE Transactions on Signal Processing*, 2016, **64** (19), pp.5145–5157

28 Feng, W., Guo, Y., Zhang, Y., Gong, J.:'Airborne radar space time adaptive processing based on atomic norm minimization', *Signal Processing*, 2018, **148**, pp.31–40

29 Yang, Z., Xie, L., Stoica, P.:'Vandermonde decomposition of multilevel Toeplitz matrices with application to multidimensional super-resolution', *IEEE Transactions on Information Theory*, 2016, **62** (2), pp.3685–3701

30 Wojaczek, P., Colone, F., Cristallini, D., Lombardo, P.:'Reciprocal Filter-based STAP for Passive Radar on moving platforms', *IEEE Transactions on Aerospace and Electronic Systems*, 2018, in press

31 Glende, M.:'PCL-signal-processing for sidelobe reduction in case of Periodical Illuminator Signals', Proc. IEEE Radar Symposium, May 2006, pp. 1–4

32 Mohimani, H., Babaie-Zadeh, M., Jutten, C.:'A Fast Approach for Overcomplete Sparse Decomposition Based on Smoothed ℓ^0 Norm', *IEEE Transactions on Signal Processing*, 2009, **57** (1), pp.289–301

33 Tropp, J.A., Gilbert, A.C.:'Signal recovery from random measurements via orthogonal matching pursuit', *IEEE Transactions on information theory*, 2007, **53** (12), pp.4655–4666
34 Chi, Y., Scharf, L.L., Pezeshki, A., Calderbank, A.R.:'Sensitivity to basis mismatch in compressed sensing', *IEEE Transactions on Signal Processing*, 2011, **59** (5), pp.2182–2195
35 Bai, G., Tao, R., Zhao, J., Bai, X.:'Parameter-searched OMP method for eliminating basis mismatch in space-time spectrum estimation', *Signal Processing*, 2017, **138**, pp.11–15
36 Feng, W., Yi, L., Sato, M.:'Near range radar imaging based on block sparsity and cross-correlation fusion algorithm', *IEEE Journal of Selected Topics in Applied Earth Observations and Remote Sensing*, 2018, **11** (6), pp.2079–2089
37 Yang, Z., Xie, L.:'Frequency-selective Vandermonde decomposition of Toeplitz matrices with applications', *Signal Processing*, 2018, **142**, pp.157–167